Electronic structures and surface states of ZnO finite well structures

2008 J. Phys. D: Appl. Phys. 41 215307

(http://iopscience.iop.org/0022-3727/41/21/215307)

IOP PUBLISHING JOURNAL OF PHYSICS D: APPLIED PHYSICS

J. Phys. D: Appl. Phys. **41** (2008) 215307 (6pp) doi:10.1088/0022-3727/41/21/215307

Electronic structures and surface states of ZnO finite well structures

Kuo-Feng Lin and Wen-Feng Hsieh[1]

Department of Photonics and Institute of Electro-Optical Engineering, National Chiao Tung University, 1001 Tahsueh Road, Hsinchu 30050, Taiwan, Republic of China

E-mail: wfhsieh@mail.nctu.edu.tw

Received 18 May 2008, in final form 18 September 2008
Published 15 October 2008
Online at stacks.iop.org/JPhysD/41/215307

Abstract

Electronic band structures and surface states were investigated for ZnO finite wells or slabs grown along $\langle 0\,0\,0\,1\rangle$ and $\langle 1\,-1\,0\,0\rangle$ directions using tight-binding representation. The dangling bonds on two end-surfaces caused surface bands for different direction grown slabs, of which the wavefunctions tend to localize at the end-surfaces. The increasing splitting of the degenerate surface bands at the Γ point was observed to decrease with the thickness of the nonpolar $[1\,-1\,0\,0]$ slab. And the quantum confinement effect is distinctively enhanced by the extra electron field induced in the $\langle 0\,0\,0\,1\rangle$ grown finite well with the polar end-surfaces.

1. Introduction

Zinc oxide (ZnO) is a promising material due to its large direct band gap (3.37 eV) and large exciton binding energy of 60 meV [1], all of which are advantageous for short-wavelength light-emitting diode [2, 3] and low-threshold laser [4, 5] applications at room temperature. It is known that the optical properties and the performance of a photonic device are mainly determined by its electronic density of states (DOS), which can be modified by the quantum confinement effects. ZnO nanostructures have superior optical properties over its bulk crystal; for instance, low-dimensional ZnO nanostructures, such as quantum dots (QDs) [6–8], nanoparticles [9, 10], nanobelts [11], nanowires [12, 13] and quantum wells [14, 15], have been widely investigated. In particular, the quantum confinement [16–19] leads to the band gap and the effective masses of electron and hole having a strong dependence on the size. Another difference which was found was that the intensity of the below-band-gap emission relative to that of the band-edge emission increases as the crystalline size decreases. Recently, Shalish *et al* [20] showed that the intensity ratio of the below-band-gap (surface state) and the band-edge luminescence in ZnO nanowires depends on the wire radius. The weight of this surface luminescence increases as the wire radius decreases at the expense of the band-edge emission. Pan *et al* [21] also predicted a significant increase in the intensity ratio of the deep level to the near band-edge emission with ever-increasing nanorod surface-aspect ratio. Thus, in quantum size nanostructures, the surface recombination may entirely quench band-to-band recombination, presenting an efficient sink for charge carriers that unless deactivated may be detrimental for electronic devices. Nevertheless, there is still a lack of a theoretical study on the influences of the crystalline size on the electronic structure and surface states in ZnO.

In comparison with simulation methods for nanostructures, the application of the *ab initio* calculation, a self-consistent method such as using local density approximation (LDA), to study electronic band structures of nanostructures or disordered alloys generally requires using very large supercells in order to mimic the distribution of local chemical environments. It is very computationally demanding. On the other hand, the tight-binding (TB) theory is a versatile and simple method to calculate the electronic properties of solids. Additionally, due to the transferability of the TB parameters, the method has been readily applied to systems with broken translational invariance such as low-dimensional structures [29, 30], clusters [31, 32] and alloys [24, 33]. Accordingly, in this paper, we used the TB method to investigate the electronic structure and surface states of ZnO finite well structures considering non-relaxed and non-reconstructed surfaces along $\langle 0\,0\,0\,1\rangle$ and $\langle 1\,-1\,0\,0\rangle$ growth directions.

2. Computation method and parameters

ZnO has the wurtzite structure semiconductors which are the layered materials, in which cation and anion layers alternate

[1] Author to whom any correspondence should be addressed.

Table 1. TB parameters (in eV) and lattice parameters (in Å) for bulk ZnO.

E(s, a)	E(p, a)	E(s, c)	E(p, c)	V(ssσ)	V(spσ)	V(psσ)	V(ppπ)	V(ppσ)	a	c
−19.046	4.142	1.666	12.368	−6.043	7.157	10.578	4.703	8.634	3.249	5.21

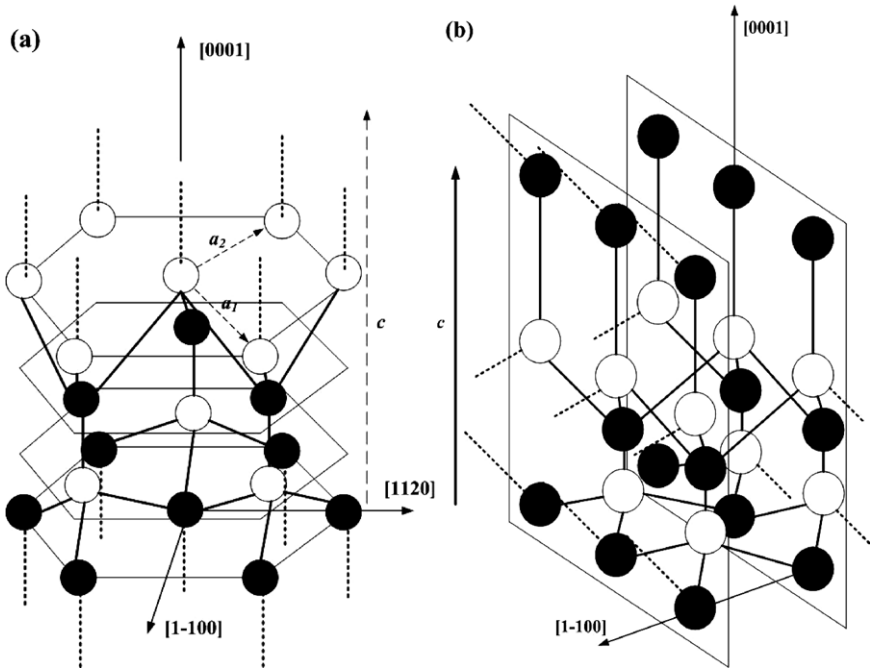

Figure 1. Finite well structures of wurtzite material. (*a*) The slab of one layer grown along the [0 0 0 1] direction. (*b*) The slab of two layers grown along the [1 −1 0 0] direction. $a1$, $a2$ and c are the unit vectors in a unit cell; dashed lines represent dangling bonds on surfaces; open and closed circles show the cation and anion atoms, respectively.

on the {0 0 0 1} planes. The unit cell of wurtzites is built on the unit vectors $\vec{a}_1 = (\sqrt{3}a/2, -a/2, 0)$, $\vec{a}_2 = (0, a, 0)$ and $\vec{c} = (0, 0, c)$, consisting of two cations and two anions. We used a semi-empirical tight-binding (SETB) method with a sp^3 basis set [22–24], which has been proven suitable for bulk wurtzite crystals. In the present calculations, the four nearest neighbour atoms are considered equivalent, even though the crystal is not cubic. The small crystal-field splittings which differentiate the p_z orbital from the $p_{x,y}$ orbitals are neglected. Under such an approximation, on-site coupling between s and p_z orbitals can also be neglected. Thus, the model has nine independent parameters including four on-site matrix elements: E(s, a), E(p, a), E(s, c) and E(p, c) (where s and p refer to the basis states and a and c refer to anion and cation) and five nearest-neighbour transfer matrix elements V(ssσ), V(spσ), V(psσ), V(ppπ) and $V(pp\sigma)$, where the first and second indices refer to anion and cation with σ and π bondings. We used the TB parameters from [22] in our numerical calculation which along with the lattice parameters a and c are listed in table 1.

Let us first consider the finite well structures grown along the ⟨0 0 0 1⟩ direction or called the [0 0 0 1] slab; the atoms in each of the layers are arranged in a hexagonal lattice with the unit cell defined by vectors $\vec{a}_1$ and $\vec{a}_2$. We assume that the layer is infinitely large and its structure is perfect (no reconstruction and relaxation on the end surfaces). As reported in [34], surface reconstruction occurs on the (1 −1 0 0) surface but not on the (0 0 0 −1) O-terminated surface and Zn vacancy on the (0 0 0 1) surface of ZnO films, while Jedrecy *et al* [35] reveal only a small atom position shift on the nonpolar surface. Therefore, it is believable to omit the effect of surface reconstruction. We can see from figure 1(*a*) that the distance between the identical successive layers in such a structure is equal to c, so that the unit cell consists of four sublayers: two cation layers and two anion layers. Therefore, the wave function should be written as a superposition of the localized cation, $\phi_\alpha^{\rm ci}$, and anion, $\phi_\alpha^{\rm ai}$, atomic orbitals $\alpha = $ s, p_x , p_y , p_z in each sublayer:

$$\Psi(\vec{r}) = \frac{1}{\sqrt{N}} \sum_{\alpha,\vec{R},l} e^{i\vec{k}\cdot\vec{R}} [A_{\alpha,l}\phi_\alpha^{\rm c1}(\vec{r}-\vec{R}) + B_{\alpha,l}\phi_\alpha^{\rm a1}(\vec{r}-\vec{R}) + C_{\alpha,l}\phi_\alpha^{\rm c2}(\vec{r}-\vec{R}) + D_{\alpha,l}\phi_\alpha^{\rm a2}(\vec{r}-\vec{R})]. \quad (1)$$

Here $A_{\alpha,l}$, $B_{\alpha,l}$, $C_{\alpha,l}$ and $D_{\alpha,l}$ describe the amplitude of the atomic orbitals in each sublayer of the lth unit cell, N is the number of unit cells in each sublayer, $\vec{R} = n_1\vec{a}_1 + n_2\vec{a}_2$ ($n_{1,2}$ are integers) is the lattice vector in the plane of each sublayer and $\vec{k}$ is the momentum lying in the hexagonal surface Brillouin zone defined by reciprocal vectors $\vec{b}_1 = 2\pi/a(2/\sqrt{3}, 0)$ and $\vec{b}_2 = 2\pi/a(1/\sqrt{3}, 1)$. In the nearest-neighbour approximation, the band structure of such a layered structure is determined by the

following matrix equation:

$$\begin{pmatrix} h_{\rm c}^0 - EI & h_{\rm ca}^+ & 0 & 0 & 0 & \cdots & 0 & 0 \\ h_{\rm ca} & h_{\rm a}^0 - EI & h_{\rm ac} & 0 & 0 & \cdots & 0 & 0 \\ 0 & h_{\rm ac}^+ & h_{\rm c}^0 - EI & h_{\rm ca}^{0+} & 0 & \cdots & 0 & 0 \\ 0 & 0 & h_{\rm ca}^0 & h_{\rm a}^0 - EI & h_{\rm ac} & \cdots & 0 & 0 \\ \vdots & \vdots & \vdots & \vdots & \vdots & \vdots & \vdots & \vdots \\ \vdots & \vdots & \vdots & \vdots & \vdots & \vdots & \vdots & \vdots \\ 0 & 0 & 0 & 0 & \cdots & h_{\rm ac}^+ & h_{\rm c}^0 - EI & h_{\rm ca}^{0+} \\ 0 & 0 & 0 & 0 & \cdots & 0 & h_{\rm ca}^0 & h_{\rm a}^0 - EI \end{pmatrix} \times \begin{pmatrix} A_1 \\ B_1 \\ C_1 \\ D_1 \\ \vdots \\ C_L \\ D_L \end{pmatrix}. \tag{2}$$

In the TB basis used each block h represents a 4×4 matrix, I is the identity matrix and A_l, B_l, C_l and D_l are the column vectors of size 4. The coupling matrices h are determined by the empirical parameters of the model and the wave vector $\vec{k}$. $h_{\rm c,a}^0$ describe on-site coupling in the anion or cation layer; $h_{\rm ca}^0$, $h_{\rm ac}$ and $h_{\rm ca}$ describe interlayer coupling.

We also consider another case that the well is grown along $\langle 1\,{-}1\,0\,0\rangle$ and represents the structure of a wurtzite crystal as a $[1\,{-}1\,0\,0]$ slab. Each surface atom forms one dangling bond tilted to the end-surface as shown in figure 1(b). The separation between equivalent layers in such a structure is equal to $\sqrt{3}a/2$, so that the unit cell includes two sublayers. In turn, the atoms in each sublayer are arranged in a rectangular lattice with a unit cell defined by the vectors $\vec{a}_1 + \vec{a}_2$ and $\vec{c}$. The surface unit cell includes two atoms, one cation and one anion, which are shifted with respect to each other by the vector $\vec{\tau} = (3/8)\vec{c}$. Therefore, in terms of the nearest neighbours, the $[1\,{-}1\,0\,0]$ surface can be represented as cation–anion dimmers directed along the $\langle 0\,0\,0\,1\rangle$ axis. Thus, the wave function of the wurtzite structure perpendicular to the axis $\langle 1\,{-}1\,0\,0\rangle$ should be written as a superposition of the localized cation and anion atomic orbitals in the lth layer including two sublayers:

$$\Psi(\vec{r}) = \frac{1}{\sqrt{N}} \sum_{\alpha,\vec{R},l} {\rm e}^{{\rm i}\vec{k}\cdot\vec{R}} [A_{\alpha,l}^{\rm c} \phi_\alpha^{\rm c1}(\vec{r} - \vec{R}) + A_{\alpha,l}^{a} {\rm e}^{{\rm i}\vec{k}\cdot\vec{\tau}} \phi_\alpha^{a1} \times (\vec{r} - \vec{R} - \vec{\tau}) + B_{\alpha,l}^{\rm c} \phi_\alpha^{\rm c2}(\vec{r} - \vec{R}) + B_{\alpha,l}^{a} {\rm e}^{{\rm i}\vec{k}\cdot\vec{\tau}} \phi_\alpha^{a1}(\vec{r} - \vec{R} - \vec{\tau})], \tag{3}$$

where the vector $\vec{R} = n_1(\vec{a}_1 + \vec{a}_2) + n_2\vec{c}$ runs over the lattice sites in each sublayer, the momentum $\vec{k}$ lies in the rectangular surface Brillouin zone built on the reciprocal vectors $\vec{b}_1 = 2\pi/a(1, 0)$ and $\vec{b}_2 = 2\pi/a(0, 1)$ and the indices $\vec{c}$ and $\vec{a}$ in the amplitudes A and B refer to cation and anion atoms in each sublayer, respectively. The formal eigenvalue problem for such an infinitely long layered structure is reduced to

$$\begin{pmatrix} H_0 - EI & H_{01} & 0 & 0 & 0 & \cdots & 0 & 0 & 0 \\ H_{01}^+ & H_0 - EI & H_{10}^+ & 0 & 0 & \cdots & 0 & 0 & 0 \\ 0 & H_{01} & H_0 - EI & H_{01} & 0 & \cdots & 0 & 0 & 0 \\ 0 & 0 & H_{01}^+ & H_0 - EI & H_{10}^+ & \cdots & 0 & 0 & 0 \\ \vdots & \vdots & \vdots & \vdots & \vdots & \ddots & \vdots & \vdots & \vdots \\ 0 & 0 & 0 & 0 & 0 & \cdots & H_{01} & H_0 - EI & H_{01} \\ 0 & 0 & 0 & 0 & 0 & \cdots & 0 & H_{01}^+ & H_0 - EI \end{pmatrix} \times \begin{pmatrix} A_1 \\ B_1 \\ A_2 \\ B_2 \\ \vdots \\ A_L \\ B_L \end{pmatrix}. \tag{4}$$

Here we defined $8 \times 8H$ matrices as

$$H_0 = \begin{pmatrix} h_{\rm c}^0 & h_{\rm ca}^0 \\ h_{\rm ca}^{0+} & h_{\rm a}^0 \end{pmatrix}, \qquad H_{01} = \begin{pmatrix} 0 & h_{\rm ca} \\ h_{\rm ac} & 0 \end{pmatrix}, \qquad H_{01} = \begin{pmatrix} 0 & \tilde{h}_{\rm ca} \\ \tilde{h}_{\rm ac} & 0 \end{pmatrix}. \tag{5}$$

The matrices h depend on the surface wave vector $\vec{k}$, which lies in the rectangular surface Brillouin zone in this case. Hence, the coupling matrices h are not identical to the h matrices for the $[0\,0\,0\,1]$ surface in equation (2). $h_{\rm c,a}^0$ describes on-site coupling in the anion or cation layer; $h_{\rm ca}^0$, $h_{\rm ac}$ and $h_{\rm ca}$ describe inter-sub-layer coupling in one layer; $\tilde{h}_{\rm ac}$, and $\tilde{h}_{\rm ca}$ describe the inter-sub-layer coupling between two layers. Therefore, we solved the eigenvalue problem of (2) and (4) to obtain electronic behaviour for ZnO finite well structures.

3. Results and discussion

3.1. Band structures for $\langle 0\,0\,0\,1\rangle$ *and* $\langle 1\,-\,1\,0\,0\rangle$ *directions*

In figures 2(a) and (b), we overlaid the band structures (solid curves) of the five-layers $[0\,0\,0\,1]$ and $[1\,{-}1\,0\,0]$ ZnO slabs, respectively, on the projected band structures (shaded regions) of bulk crystal using the approach described in [25]. The extrema of the conduction and the valence bands of the bulk ZnO are found to be $E_c = 3.36\,{\rm eV}$ and $E_v = 0\,{\rm eV}$, respectively. We also used the transfer matrix method [25, 26] to prove that the dangling bonds of the cations (Zn) result in a surface band as a solid curve close to the bottom of the conduction band in figure 2(a), while the dangling bonds of the anions (O) give rise to the surface bands near the middle of the band gap (around 1.3 eV). This is in agreement with the origin of the conduction (valence) band mostly from the cation (anion) atomic orbitals [22, 24]. We also perceived that there are energy dips at the midst of the band gap for the oxide-settled surface bands at the Γ point. The depth of the energy dip is dependent on the slab thickness that may be caused by coupling between the O- and Zn-terminated surfaces. A further study to clarify this problem is required and is under way. In figure 2(b), we can see that the band gap of the slab is formed by four bands, which include two bands slightly above the bottom of conduction band and the other two bands in the middle of the band gap at the Γ point. In particular, we observed the

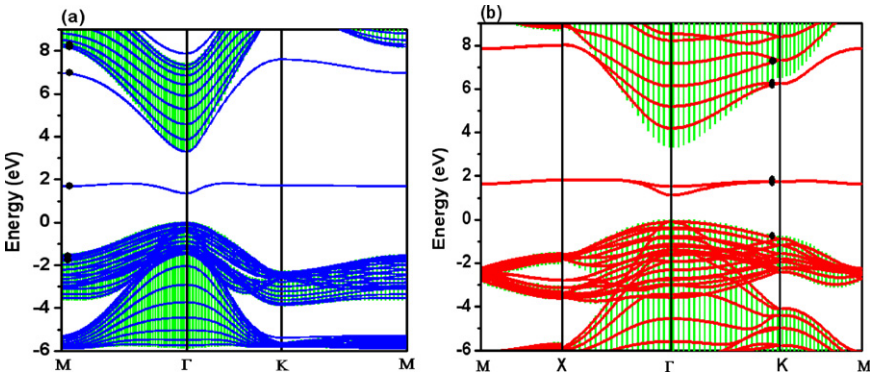

Figure 2. The band structures of the ZnO slabs with five layers along (*a*) [0 0 0 1] and (*b*) [1 −1 0 0]. The solid curves are the surface states and the shaded regions show the projected band structure of the bulk.
(This figure is in colour only in the electronic version)

splitting of these bands around the neighbourhood of the Γ point and the difference between the near-conduction bands and the middle-gap bands decreases with the increase in the slab thickness. On the other hand, there is strong coupling between the surface states with the allowed bands, especially at the Γ point. In order to reduce these coupling effects, we calculated the wave functions for the parallel (to the layers of the well) wave vector, $k_{||}$, away from the Γ point for ensuring accurate characterizing of the properties of surface states.

3.2. Wave function and quantum effect for ZnO finite well

The wave functions $|\Psi|$ of the six bands for the [0 0 0 1] slab of five layers close to the M point labelled in figure 2(*a*) are shown in ascending energy order in figure 3(*b*). And the wave functions with the same $k_{||}$ for the two and ten layer slabs were also plotted in figures 3(*a*) and (*c*), respectively. On analysing the wave functions across the [0 0 0 1] slabs in figures 3(*a*)–(*c*), we can see that the bands (the first and second bands) near the conduction band edge are mainly contributed by cation layers with high $|\Psi|$ being located at the cation sites, and the upper valence bands (the fifth and sixth bands) are mainly contributed by the anion layers with high $|\Psi|$ being located at the anion sites. It is observed that the wave function (the third curve) of the closest (surface) band to the conduction band edge is localized in the top cation-terminated layer and the surface band at the midgap (∼1.3 eV) is localized in the bottom anion-terminated layer. Our calculations are consistent with the results of Kresse *et al* [27] which calculated the Zn-terminated surface and the O-terminated surface using the density-functional theory.

Similarly, in order to eliminate the strong coupling between the surface states with the allowed bands close to the Γ point we plotted the wavefunctions of the [1 −1 0 0] slabs with thickness $L = 2$, 5 and 10 layers near the K point in figures 3(*d*)–(*f*). We can see that besides the wavefunctions of these two midgap bands (the second and the third) there are two other bands (the fourth curves the fifth curves) which show a tendency towards surface localization. Theoretically [28], these four bands should be considered as surface bands induced by the dangling bonds, in contrast to the allowed bands induced by the atoms in the interior layers (the first and the sixth bands).

The surface state is induced by each dangling bond in a unit cell of the end-surface. The coupling of the degenerate surface states on the periodic surface generates a surface band in the surface Brillouin zone. Furthermore, the coupling between these two identical end-surfaces sandwiching the slab causes their degenerate bands to split into symmetrical and antisymmetrical bands. A larger overlap of the wave functions of the degenerate bands will cause a larger energy splitting. As a result, the splitting of the degenerate surface bands increases with the decrease in the thickness of the slab. However, the energy splitting will not be perceived for the [0 0 0 1] slabs, since the polar end-surfaces are not identical. Another important consequence is that the splitting at the Γ point is the largest in comparison with that at the other Brillouin-zone boundaries. As in figure 2(*b*) of the five layers [1 −1 0 0] slab, the two higher surface bands near the Γ point embed themselves in the conduction band of the bulk. These bands are as expected toward the conduction band edge of the bulk with increasing L. In general, the localization length of the surface state is inversely proportional to its energy separation from the related allowed band. Since the surface bands more closely approach the allowed conduction and valence bands near the Γ point, their localization length must be longer at the Γ point than at the other $k_{||}$ in the Brillouin zone. A larger localization length at the Γ point results in a larger overlap between the degenerate surface states, which explains the largest splitting of the bands at the Γ point. Additionally, we noted in figure 4 that the edges of conduction and valence bands shift towards each other so that the bandgap decreases with increasing L. As a matter of fact, this is a direct evidence of the quantum size effect. Obviously, the quantum size effect of the [0 0 0 1] slabs was more apparent than that of the [1 −1 0 0] slabs due to the polar surface induced extra electron field which enhanced the quantum confinement effect for the [0 0 0 1] slabs. And both the band structure of the slab and the surface bands become similar to those of the semi-infinite crystal with the increase in the number of layers and the bands finally bundle to form the band spectrum of the bulk.

We also included data of our previous experimental results (hollow circle point) of quantum size effects from passivated ZnO QDs [17] in figure 4 for a comparison even though they are QDs rather than quantum wells. It indicated that

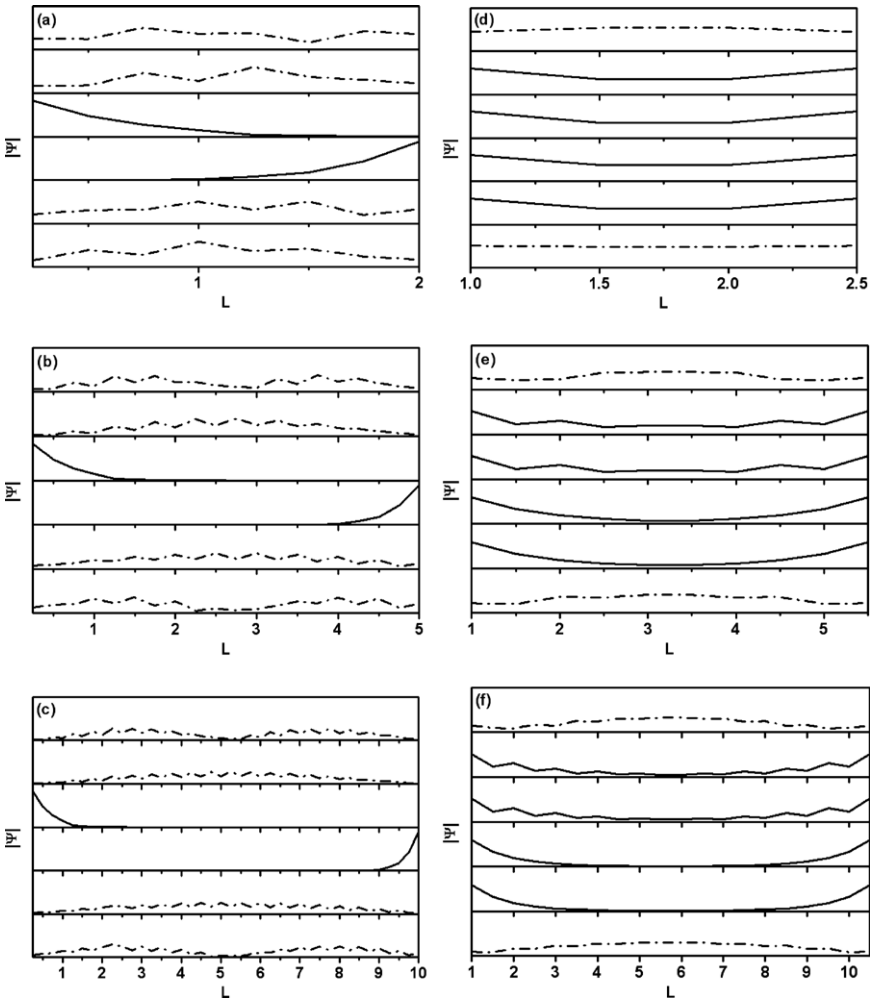

Figure 3. The wave functions of the six bands closest to the middle of the band gap away from the Γ point for the slabs of two, five and ten layers along [0 0 0 1] (*a*)–(*c*) and along [1 −1 0 0] (*d*)–(*f*).

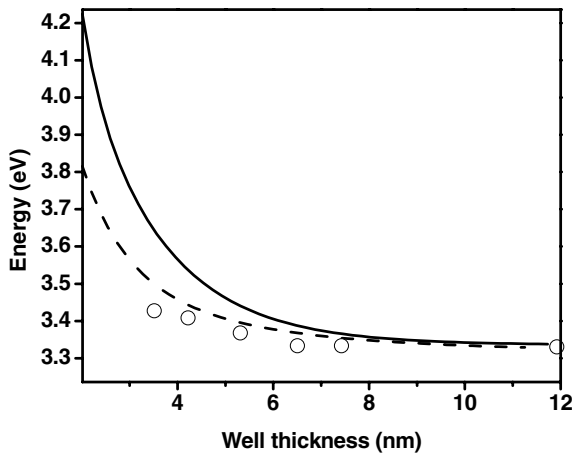

Figure 4. Variations of the band gap as a function of the thickness for ZnO well along [0 0 0 1] (solid curve), [1 −1 0 0] (dashed curve) directions and experiment data (hollow circle point).

our experimental results reasonably match with the calculated bandgap energy along the [1 −1 0 0] direction, which is quite reasonable because the polar surfaces only appear along the [0 0 0 1] direction and have less contribution to near band edge emission. Because the surface was passivated by hydroxide in our samples, our experiment data displayed minimal surface state emission to bring out the blue shifted near band-edge emission resulting from the quantum size effects.

4. Conclusion

In conclusion, using tight-binding representation of the layered systems grown along ⟨0 0 0 1⟩ and ⟨1 −1 0 0⟩ directions, we calculated the band structures and wave functions for various ZnO slab layers with non-relaxed and non-reconstructed surfaces. We show that dangling bonds on the two end-surfaces cause surface bands for different direction-grown slabs. On analysing the wave functions across the layers, the surface states show a tendency towards surface localization. In particular, the splitting of the degenerate surface bands increases due to increasing overlap between their wave functions, which are localized on two nonpolar [1 −1 0 0] end-surfaces, while it is not present for the [0 0 0 1] finite well with polar end-surfaces. Finally, we also found that the quantum confinement effect is effectively enhance due to the extra electron field along the [0 0 0 1] polar end-surfaces.

Acknowledgments

This work was partially supported by the National Science Council and the Ministry of Economic of the Republic of China under Contract No NSC 96-2628-M-009-001-MY3.

References

[1] Hümmer K 1973 *Phys. Status Solidi* b **56** 249
[2] Nadarajah A, Word R C, Meiss J and Konenkamp R 2008 *Nano Lett.* **8** 534
[3] Sun H, Zhang Q, Zhang J, Deng T and Wu J 2008 *Appl. Phys.* B **90** 543
[4] Emel'chenko G A, Gruzintsev A N, Kulakov A B, Samarov E N, Karpov I A, Red'kin A N, Yakimov E E and Barthou C 2007 *Semiconductors* **41** 176
[5] Bouvy C, Chelnokov E, Zhao R, Marine W, Sporken R and Su B L 2008 *Nanotechnology* **19** 105710
[6] Fonoberov V A and Balandin A 2004 *Appl. Phys. Lett.* **85** 5971
[7] Cheng H M, Lin K F, Hsu H C and Hsieh W F 2006 *Appl. Phys. Lett.* **88** 261909
[8] Lin K F, Cheng H M, Hsu H C and Hsieh W F 2006 *Appl. Phys. Lett.* **88** 263117
[9] Pan C J, Lin K F, Hsu W T and Hsieh W F 2007 *J. Appl. Phys.* **102** 123504
[10] Pan C J, Lin K F and Hsieh W F 2007 *Appl. Phys. Lett.* **91** 111907
[11] Pan Z W, Dai Z R and Wang Z L 2001 *Science* **291** 1947
[12] Huang M H, Mao S, Feick H, Yan H, Wu Y, Kind H, Weber E, Russo R and Yang P 2001 *Science* **292** 1897
[13] Hsu H C, Wu C Y and Hsieh W F 2007 *J. Appl. Phys.* **97** 064315
[14] Lim J H, Kang C K, Kim K K, Park I K, Hwang D K and Park S J 2006 *Adv. Mater.* **18** 2720
[15] Bae J Y, Yoo J and Yi G C 2006 *Appl. Phys. Lett.* **89** 173114
[16] Gudiksen M S, Wang J and Lieber C M 2002 *J. Phys. Chem.* B **106** 4036
[17] Lin K F, Cheng H M, Hsu H C, Lin L J and Hsieh W F 2005 *Chem. Phys. Lett.* **409** 208
[18] Maslov A V and Ning C Z 2005 *Phys. Rev.* B **72** 125319
[19] Hsu W T, Lin K F and Hsieh W F 2007 *Appl. Phys. Lett.* **91** 181913
[20] Shalish I, Temkin H and Narayanamurti V 2004 *Phys. Rev.* B **69** 245401
[21] Pan N, Wang X, Li M, Li F and Hou J G 2007 *J. Phys. Chem.* C **111** 17265
[22] Kobayashi A, Sankey O F, Volz S M and Dow J D 1983 *Phys. Rev.* B **28** 935
[23] Jenkins D W and Dow J D 1989 *Phys. Rev.* B **39** 3317
[24] Lin K F, Pan C J and Hsieh W F 2008 *Appl. Phys.* A submitted
[25] Lee D H and Joannopoulos J D 1981 *Phys. Rev.* B **23** 4988
[26] Malkova N and Ning C Z 2006 *Phys. Rev.* B **74** 155308
[27] Kresse G, Dulub O and Diebold U 2003 *Phys. Rev.* B **68** 245409
[28] Many A, Goldstein Y and Grover N B 1965 *Semiconductor Surfaces* (North-Holland, Amsterdam)
[29] Allan G and Delerue C 2004 *Phys. Rev.* B **70** 245321
[30] Leung K, Pokrant S and Whaley K B 1998 *Phys. Rev.* B **57** 12291
[31] Schulz S and Czycholl G 2005 *Phys. Rev.* B **72** 165317
[32] Schulz S, Schumacher S and Czycholl G 2006 *Phys. Rev.* B **73** 245327
[33] Jenkins D W and Dow J D 1989 *Phys. Rev.* B **39** 3317
[34] Ding Y and Wang 2007 *Surf. Sci.* **601** 425
[35] Jedrecy N, Gallini S, Sauvage-Simkin M and Pinchaux R 2000 *Surf. Scien.* **463** 136